In-situ and Ex-situ Processes for Synthesizing Metal Multilayers with Electronically Conductive Interfaces

Frank Angeles[1], Xinping Shi[1], Richard B. Wilson[1,2]

1) Mechanical Engineering, University of California, Riverside, CA, 92507, USA
2) Material Science and Engineering, University of California, Riverside, CA, 92507, USA

Abstract

A number of technological applications and scientific experiments require processes for preparing metal multilayers with electronically and thermally conductive interfaces. We investigate how *in-situ* vs. *ex-situ* synthesis processes effect the thermal conductance of metal/metal interfaces. We use time-domain thermoreflectance experiments to study thermal transport in Au/Fe, Al/Cu, and Cu/Pt bilayer samples. We quantify the effect of exposing the bottom metal layer to an ambient environment prior to deposition of the top metal layer. We observe that for Au/Fe, exposure of the Fe layer to air before depositing the top Au layer significantly impedes interfacial electronic currents. Exposing Cu to air prior to depositing an Al layer effectively eliminates interfacial electronic heat-currents between the two metal layers. Exposure to air appears to have no effect on interfacial transport in the Cu/Pt system. Finally, we show that a short RF sputter etch of the bottom layer surface is sufficient to ensure a thermally and electronically conductive metal/metal interface in all materials we study. We analyze our results with a two-temperature model and bound the electronic interface conductance for the nine samples we study. Our findings have applications for thin-film synthesis and advance fundamental understanding of electronic thermal conductance at different types of interfaces between metals.

1. Introduction

Interfaces govern thermal and electrical transport in nanostructured materials and devices [1]. Low resistance interfaces are important for applications that require efficient heat dissipation, such as microelectronic semiconductor devices [2]. The ability to synthesize metal multilayers with thermally and electrically conductive interfaces is also important for a number of scientific experiments. These include ultrafast optical thermometry [3], spin caloritronic studies [4][5][6], as well as femto-magnetism and ultrafast spintronics studies[7][8][9][10][11].

Thermal transport at interfaces is characterized by the interfacial thermal resistance R, which linearly relates the temperature drop ΔT at the interface to the heat-current $J = \Delta T/R$ across the interface [12]. The inverse of the interfacial thermal resistance is the thermal boundary conductance $G = 1/R$. The interfacial thermal resistance is caused by scattering of heat carriers. In metals, heat is carried by electrons. In non-metals, heat is carried by phonons.

Interfaces between metals can be significantly more heat conductive than interfaces between insulators. The largest thermal interface conductance reported to date is for an interface between

Pd and Ir with G ~ 14 GW m−2 K−1 [13]. Reported values for the thermal conductance at metal/metal interfaces range from 0.5 to 14 GW m^{-2} K^{-1} [1][14][15][16][17]. Alternatively, when heat is carried across an interface by phonons instead of electrons, the interface is typically at least an order of magnitude less conductive. Reported values for *G* of metal/insulator or metal/semiconductor interfaces range from 0.01 to 1 GW m^{-2} K^{-1} [18][19][20][21][22].

For metal interfaces to be thermally conductive, electrons need to be able to easily traverse the interface. Oxide layers, or other interfacial disorder that is electrically resistive, can prevent electrons from traversing the interface. Jang et al. report that a 2 nm interlayer of MgO or $MgAl_2O_3$ between Ru and Co results in an interface conductance of ≈ 0.2 – 0.3 GW m^{-2} K^{-1}. This value is an order of magnitude lower than is observed for metal/metal interfaces without oxide interlayers [1][13][15]. Since there have been very few experimental studies of thermal transport at interfaces between metals with oxide-layers or interfacial disorder, there a clear understanding of how thermally conductive imperfect interfaces can be has not yet been established.

Here, we investigate how different processes for synthesizing metallic bilayers effects interfacial thermal properties. Our study has two goals. First, we want to understand what types of metals need to be deposited in-situ to ensure that the interfaces can conduct electronic heat-currents. By in-situ, we mean the sample is prepared without breaking vacuum in between deposition of the two metal layers. Second, we want to identify a process that ensures good thermal contact between two metal layers, even if they aren't prepared in-situ with each other. To accomplish this later goal, we explore the ability of RF sputter etching to clean dirty or oxidized metal surfaces prior to deposition of the top metal layer.

We prepare and characterize heat transfer in a total of nine metal bilayers. Each of our nine samples is one of three material combinations: Au/Fe, Al/Cu, and Cu/Pt. Each material combination was prepared in one of three ways. The first set of samples are prepared *in-situ*. The second set of bilayers are prepared *ex-situ*, i.e., vacuum is broken in-between the deposition of the two metal layers. Finally, the third set of samples are also prepared *ex-situ*. Then, prior to depositing the top metal layer, the bottom metal layer is RF sputter etched, *ex-situ+RF*.

The logic for these material choices was as follows. Au/Fe is a bilayer where the bottom layer oxidizes, and the top layer does not. Al/Cu is a bilayer where both top and bottom layers both oxidize. Cu/Pt is a bilayer where the bottom layer does not oxidize, and the top layer does. Therefore, these material systems allow us to investigate how a metal's propensity to form oxide layers effects thermal transport in samples prepared with *ex-situ* vs. *in-situ* processes.

We find that the interface conductance between Au/Fe and Al/Cu, interfaces are all greater than 4 GW/(m^2-K) when deposited *in-situ*. For the Cu/Pt system the interface conductance falls between 3.3 – 5.5 GW/(m^2-K). For Au/Fe and Al/Cu systems that were prepared *ex-situ*, and were also RF-sputter etched prior to the top metal deposition, we also observe *G* greater than 4 GW/(m^2-K). Alternatively, for *ex-situ* samples that were not RF sputter cleaned, we observe that *G* depends on whether the bottom layer forms a native oxide. Both Cu and Fe form oxides when exposed to air.

For *ex-situ* Al/Cu, we observe a significant reduction of $G \approx 0.065 \pm .15$ GW/(m^2-K). For *ex-situ* Au/Fe, we observe $G \approx 1.7 \pm 0.9$ GW/(m^2-K). Finally, in *ex-situ* prepared Cu/Pt we observe $G \approx 5.0 \pm 1.3$ GW/(m^2-K). We credit the high *ex-situ* Cu/Pt interfacial thermal conductance to the fact that Pt surfaces do not form oxides.

2. Experimental Methods

2.1. Sample Preparation Description

The metal films were sputter deposited using an Orion series AJA magnetron sputtering system. The base pressure of the vacuum chamber prior to DC magnetron deposition was kept bellow ~3.5e-7 torr. During deposition, the base pressure is raised to 3.5 mTorr by introducing high purity Argon via a mass flow controller. All samples are grown at room temperature on a (0001) sapphire (Al_2O_3) substrate. The Al, Cu, and Fe are sputtered from a 2-inch targets at 200 W. The Pt is sputtered from a 1-inch target at 10 W.

As described above, to investigate thermal transport across metal/oxide/metal interfaces we created three sets of samples to compare. The first type of sample we study are bilayers that are prepared via sequential *in-situ* magnetron sputter deposition of both layers. This first set of samples was sputtered without a vacuum break. As a result, we are reasonably confident there is no physically absorbed molecules or oxide layer on the surface of the bottom metal when the 2nd metal is deposited.

The second set of samples were not sputter deposited simultaneously. The first metal layer was deposited, and then taken out of the chamber and placed on a hot plate 100 C for ~10 minutes. This heat-treatment in an ambient environment was intended to help expedite any chemical reactions likely to take place during an extended exposure to air, such as an oxide layer formation at the metal surface.

The third set of samples were identical to the 2nd set described above. Except, after being placed back into the chamber, their surface was RF sputter cleaned prior to the deposition of the top metal layer. The sample stage was RF biased at 45 W for 300 seconds in an Argon plasma pressure of 3.5 mTorr. After the RF sputter etch clean, the top metal layer was sputter deposited onto the sample.

To investigate the effect of the RF etching time on thermal transport, we prepared three additional ex-situ+RF Al/Cu bilayer samples. We prepared these three additional Al/Cu samples in the same way as described above, but with the RF etch time varied. The first sample was RF etched at a power of 45 W for 10 seconds. The second sample was RF etched in a multi-stage process. The plasma was ignited at a power less than 5 W. Upon ignition of the plasma, the power was linearly ramped for 40 seconds to a power of 45 W. Then, the power was held fixed at 45 W for 30 seconds. For the third sample, we followed a similar multi-stage process as for the 2nd sample. But, after ramping, the sample was RF etched at a constant power of 45 W for 60 seconds.

2.2. Pump/Probe Experiments

We use time domain thermo-reflectance (TDTR) experiments to study thermal transport in the bilayers. We are primarily interested in the thermal interface conductance between the metals. TDTR is a well-established pump/probe technique for measuring thermal properties of thin-films and interfaces [23]. TDTR determines thermal properties by measuring the transient evolution of the surface temperature that results from heating by pump pulses. The time-evolution of the surface temperature is measured with a time-delayed probe pulse. The probe pulse detects temperature-induced changes to the sample's reflectance. The time required for the metal film to cool after being heated with the pump pulse is determined by the transport properties of the metal, including the interfacial thermal conductance between metals. The laser spot size in all our experiments was kept constant at $w_0 \approx 6.5$ μm. The pump modulation frequency in our experiments is $f = 10.7$ MHz.

In regular TDTR experiments the pump and probe are both incident on the surface of the metallic transducer. In our experiment we used a front back set up for the pump and probe, see Fig 1. This means the pump is incident on the first metallic layer through the substrate and the probe was incident on the surface of the second metallic layer. In this geometry, TDTR becomes a nanoscale laser flash measurement that measures how quickly heat takes to traverse the nanoscale metal bilayers [24].

We measure film thicknesses of our samples using picosecond acoustic signals in our TDTR data. We model acoustic wave propagation with an analytical solution to the acoustic wave equation. The model uses literature values for the density and elastic constants of metals as inputs, and treats the film thickness as a fit-parameter. We compare the predictions of the acoustic model to TDTR data after subtracting temperature-induced contributions to the signal, see Fig 2.

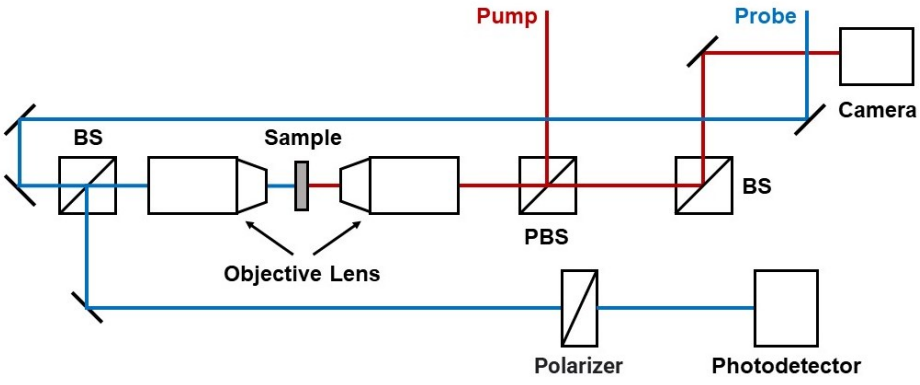

Figure 1. Schematic of the optical layout for the front-back pump–probe measurement system. Red solid line indicates pump and blue solid line indicates probe. The elements labeled PBS and BS are polarizing beam splitters and beam splitters.

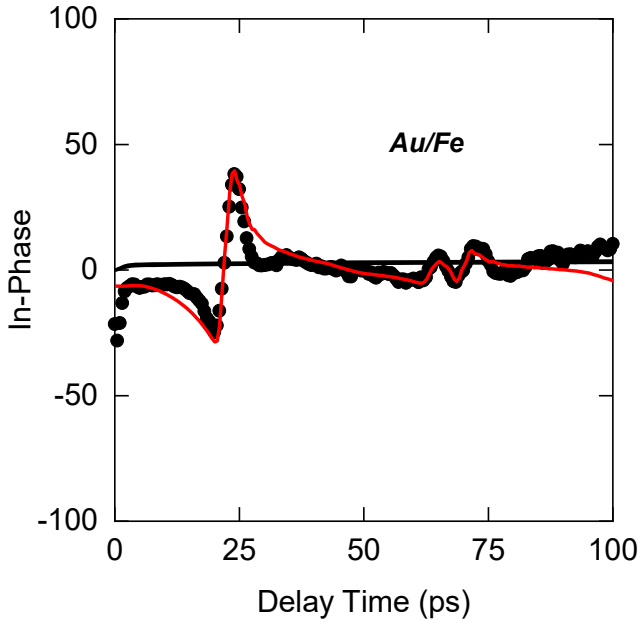

Figure 2. Picosecond acoustic data and acoustic model predictions for *in-situ* Au/Fe bilayer. The black markers show the TDTR in-phase signal vs delay time after temperature-induced contributions to the signal are subtracted out. The red line is a solution of the acoustic wave equation with Au and Fe layer thicknesses treated as fit parameters, best fit values are Au 73nm and Fe 17 nm. We used a similar analysis to determine layer thicknesses in all samples.

3. Results and Analysis

Our TDTR experiments show that the thermal response to pump heating depends on the preparation method, see Figs. 3-5. As described above, in these experiments, the heat is deposited at the bottom of the bottom metal layer, and the temperature is measured at the surface of the top metal layer. The thermal response of the top layer's surface depends on the total thermal resistance across the bilayer. This total thermal resistance includes the thermal resistance of the bottom metal layer, the interface, and the top metal layer. In metal layers with weak electron-phonon coupling, e.g. Au, the thermal resistance between electrons and phonons is also significant [24].

In all three-samples we study, the observed thermal response of *in-situ* and *ex-situ+RF* bilayer samples are similar. This is the main result of our study. RF sputtering the surface of a metal prepared ex-situ is sufficient to ensure both a thermally and electronically conductive interface.

We observe that 30 seconds of RF etching is sufficient to ensure a thermally conductive interface between Al and Cu, see Fig. 6. Al/Cu samples prepared with RF etch times of 30 and 60 seconds have interfaces that are as thermally conductive as the in-situ and ex-situ + 5-minute RF etch sample in Fig. 4. Alternatively, the Al/Cu bilayer with only 10 seconds of RF etch time has a

thermal response similar to the ex-situ Al/Cu sample. This indicates that 10 seconds is not enough to ensure a high electronic conductance between two metals.

We now discuss how *ex-situ* samples compare to the *in-situ* and *ex-situ*+RF samples. For the Au/Fe bilayer prepared *ex-situ*, the temperature rise of the Au surface is smaller than for the other two bilayers, see Fig. 3. This suggests the thermal resistance between the Fe layer and Au surface is larger in the *ex-situ* sample than in the *in-situ* or *ex-situ+RF* samples. However, the effect is small. In the Cu/Pt bilayer, the difference in the thermal response between all samples is also small, see Fig. 5.

The method of preparation has the largest effect on the thermal response of the Al/Cu bilayers. For the *in-situ* and *ex-situ+RF* samples, the Al layer heats up within a picosecond of pump heating. Alternatively, for the *ex-situ* sample, it takes hundreds of picoseconds for the Al film to heat-up. This suggests an order of magnitude change in the thermal resistance between the Cu layer and the Al surface.

In the section below, we use a two-temperature model to attempt to quantify the electron-electronic conductance of the nine samples. However, we note the experimental data in Fig. 3-5 directly addresses the two primary goals of our study without the two-temperature model analysis. Examination of Figs. 3-5 reveals that a 5-minute RF sputter etch of metals prepared *ex-situ* ensures thermally conductive metal/metal interfaces. For metals like Pt, which do not form metal-oxide, we see that RF sputtering has no observable effect on electronic interfacial transport (Fig. 5) and is not necessary. Therefore, we conclude that physisorption of molecules on the Pt surface while it is outside vacuum does not adversely affect electronic interfacial transport in the Cu/Pt *ex-situ* bilayer. The effect of *ex-situ* preparation is largest in the bilayer system where both materials form oxides, i.e. Al/Cu. *Ex-situ* preparation has a small effect on transport in the Au/Fe bilayer, where only the Fe layer forms an oxide, and the oxide is poor conductor [25].

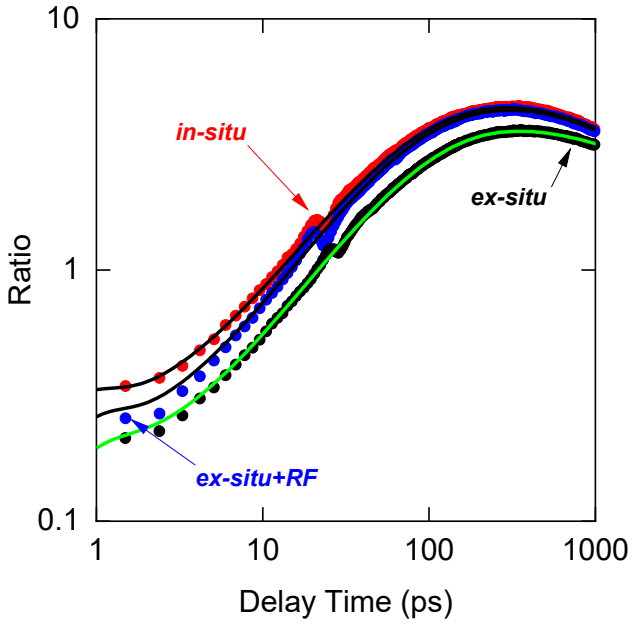

Figure 3. TDTR data for Au/Fe bilayers. Red, black, and blue markers are data for bilayers prepared *in-situ*, *ex-situ*, and *ex-situ* with RF sputtering prior to top metal layer deposition, respectively. The solid black lines are predictions of the two-temperature model with the electron-electron interface conductance set to $G_{ee} \approx 5$ GW/(m^2-K). The green solid line is a two-temperature model prediction with the electron-electron interface conductance set to $G_{ee} \approx 1.7$ GW/(m^2-K).

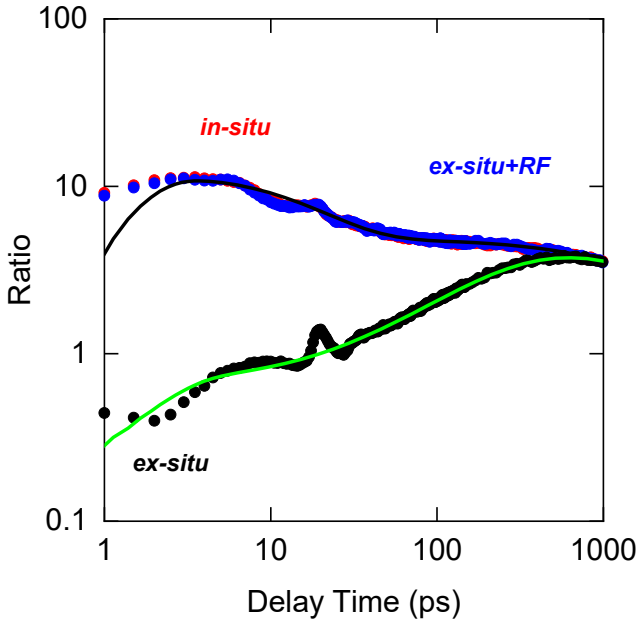

Figure 4. TDTR data for Al/Cu bilayers. Red, black, and blue markers are data for bilayers prepared *in-situ*, *ex-situ*, and *ex-situ* with RF sputtering prior to top metal layer deposition, respectively. The black solid line is a two-temperature model prediction with the electron-electron interface conductance set to $G_{ee} \approx 5$ GW/(m^2-K). The green solid line is a two-temperature model prediction with the electron-electron interface conductance set to $G_{ee} \approx 0.065$ GW/(m^2-K).

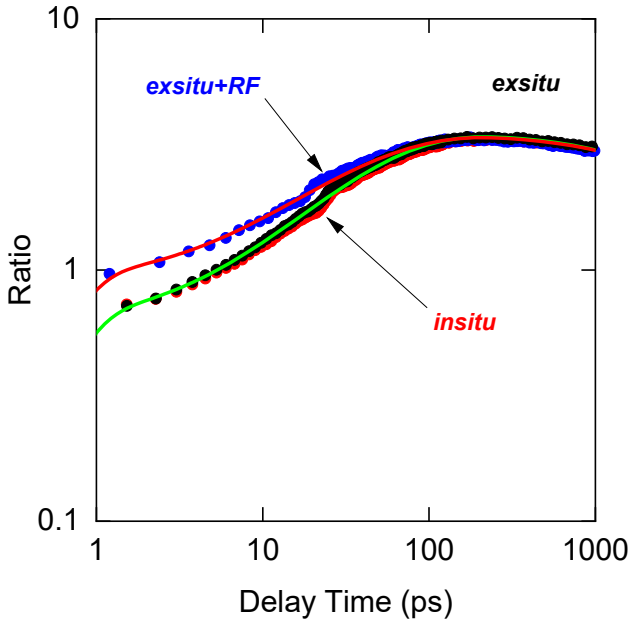

Figure 5. TDTR data for Cu/Pt bilayers. Red, black, and blue markers are data for bilayers prepared *in-situ*, *ex-situ*, and *ex-situ* with RF sputtering prior to top metal layer deposition, respectively. The red and green solid lines are two-temperature model predictions for the thermal response of the bilayer with the electron-electron interface conductance set to $G_{ee} \approx 5$ GW/(m^2-K). The difference in the two curves is that the *ex-situ* + RF bilayer has a Pt layer that is ~4.5 nm thinner.

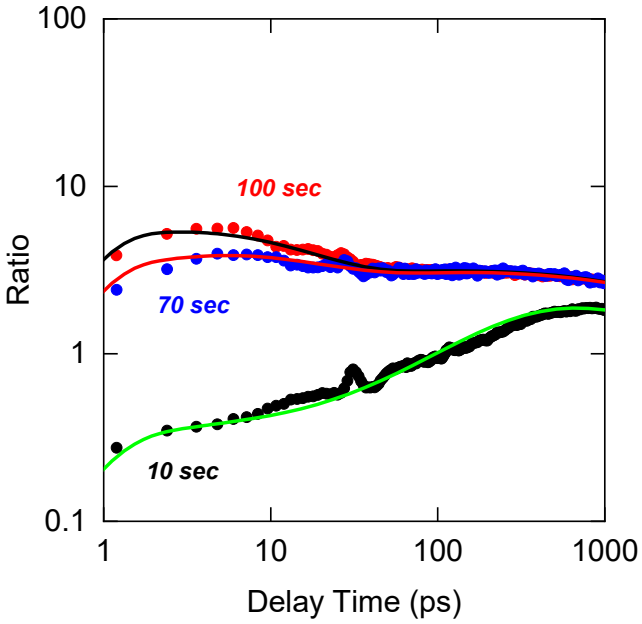

Figure 6. TDTR data for Al/Cu bilayers for different times of RF etching. Black markers are data for bilayers prepared *ex-situ* with RF sputtering. The RF sputtering time was varied for all three samples, see main text. The red, blue, and black markers correspond to total RF etch times of 100, 70, and 10 seconds. The red and black solid lines are two-temperature model predictions for the thermal response of the bilayer with the electron-electron interface conductance set to $G_{ee} \approx 5$ GW/(m^2-K). The green solid line is a two-temperature model prediction with the electron-electron interface conductance set to $G_{ee} \approx 0.150$ GW/(m^2-K).

3.1. Two Temperature Model Analysis

To quantitatively relate the observed thermal response of the bilayers to interfacial transport coefficients, we analyze our data with a two-temperature model. Our two-temperature model is a numerical solution to heat flow in a multilayer two-channel system [26]. Electrons and phonons in each layer are treated as coupled thermal reservoirs. Each thermal reservoir has its own heat-equation. In 1D, the heat equations for each channel are

$$C_{\text{ele}} \frac{\partial T_{\text{ele}}}{\partial t} = \Lambda_{\text{ele}} \frac{\partial^2 T_{\text{ele}}}{\partial z^2} - \text{g}(T_{\text{ele}} - T_{\text{ph}}),$$

$$C_{\text{ph}} \frac{\partial T_{\text{ph}}}{\partial t} = \Lambda_{\text{ph}} \frac{\partial^2 T_{\text{ph}}}{\partial z^2} + \text{g}(T_{\text{ele}} - T_{\text{ph}}),$$

Where C_{ele} and C_{ph} are specific heats of electrons and phonons, Λ_{ele} and Λ_{eph} are thermal conductivities of electrons and phonons, T_{ele} and T_{ph} are temperatures of electron and phonons, and g is energy transfer coefficient between electrons and phonons. Heat-equations between layers are coupled via electron-electron and phonon-phonon interfacial boundary conditions. The thermal network for Au/Fe system can be seen in Figure 7.

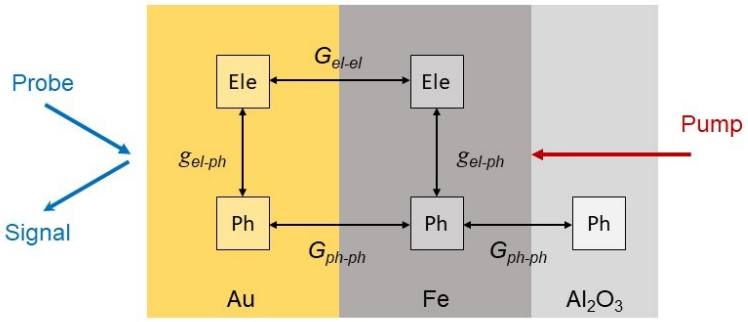

Figure 7. Device structure for Au/Fe System alongside the thermal network. The rate of heat transfer between electrons and phonons is governed by a thermal conductance per unit volume, $g_{el\text{-}ph}$. The rate of heat transfer between electrons in the Au and electrons in the Fe is governed by an electronic interfacial thermal conductance per unit area, $G_{el\text{-}el.}$ The rate of heat transfer between phonons in the Au and phonons in the Fe is governed by an interfacial thermal conductance per unit area, $G_{ph\text{-}ph.}$ The rate of heat transfer between electrons in the Au and electrons in the Pt is governed by an electronic interfacial thermal conductance per unit area, $G_{el\text{-}el.}$

The model takes the thermal properties and thickness of each layer in the system and outputs a prediction temperature for each channel i.e. electrons and phonons.

Before comparing our TDTR data and two-temperature model predictions, we need to account for a mismatch between what TDTR experiments measure and what the thermal model predicts. Our two-temperature model predicts a temperature response of the phonons and electrons as a function of time and depth. TDTR measures the thermal response of the metal bilayers through temperature induced changes in reflectance[27]. We assume TDTR signals are proportional to a weighted average of the two-temperature model predictions for the electron and phonon temperatures at the surface of the top layer. We treat the proportionality constant as a fit parameter, and set it so the model prediction and ratio data agree at 3000 ps. The relative contributions of electron and phonon temperatures to the thermoreflectance signal are also treated as a fit parameter. For example, in the Au/Fe system the phonon contribution to the model is 99% and the electron contribution is 1%.

We set most of the thermal model parameters based on independent measurements, or literature values, see Table 1. We treat the electronic and vibrational interface conductance between the two metal layers as fit parameters. We adjust these two parameters until model and data agree in the range of 1 ps up to 1000 ps.

In most of our experiments, there is a not one unique combination of electron-electron and electron-phonon conductance values that fit our data. There are a range of values we can input into the model that lead to an agreement with our data. To quantify this range of values, we calculate the root mean square percentage error (RMSE) between the data and model predictions across a wide-range of electron-electron and electron-phonon conductance values. In Fig. 8, we show contour plot illustrating all pairs of electron-electron and electron-phonon conductance that lead to a RMSE of < 7.0% for *in-situ* and *ex-situ* Au/Fe, < 5.5% for *in-situ* Al/Cu, < 16% for *ex-situ* Al/Cu, and < 4.0 % for *in-situ* and *ex-situ* Cu/Pt system. The difference in percentage arises from a minimum RMSE deviation that depends on the strength of the picosecond acoustic echoes. The effect of the picosecond echoes on the experimental signal is not included in the two-temperature model predictions, and the signal from acoustic echoes varies between samples.

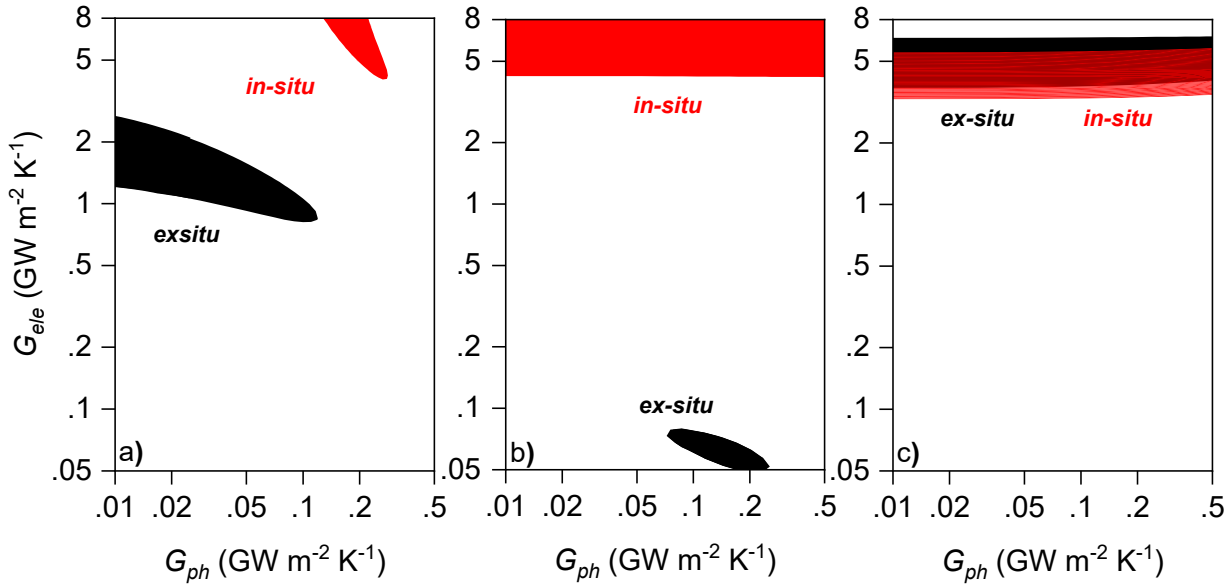

Figure 8. Contour map of the root mean square percentage error between model fits and TDTR data for a) Au/Fe bilayer, b) Al/Cu bilayer, and c) Cu/Pt bilayer. Filled areas indicate conductance values that yield two-temperature model predictions whose root mean square percentage error with TDTR data is < 7.0% for *in-situ* and *ex-situ* Au/Fe , < 5.5% for *in-situ* Al/Cu, < 16% for *ex-situ* Al/Cu, and < 4.0% for *in-situ* and *ex-situ* Cu/Pt. The red shaded region is for the *in-situ* samples. The black shaded region is for *ex-situ* samples.

3.2. Discussion

Our two-temperature model fits suggest the electron-electron interface conductance G_{ee} > 4 GW/(m^2-K) in four of the nine bilayers. These four samples include *in-situ* and *ex-situ+RF* Au/Fe and Al/Cu samples. All three of the Cu/Pt samples have electron-electron interface conductance between 3.3 < G_{ee} < 6.5 GW/(m^2-K). It is important to note that 4 GW/(m^2-K) is only a lower bound to the electronic conductance. The thermal model predictions lose sensitivity to G_{ee} when it is larger than 5 GW/(m^2-K). This is because the electron conductance stops being a significant contributor to the total thermal resistance across the bilayer. We illustrate this in Fig. 8. Fig. 8 shows the range of phonon and electron interface conductance values that yield a good fit to the a) Au/Fe TDTR data b) Al/Cu TDTR data, and c) Cu/Pt TDTR data, i.e. a root mean square percentage error less than 7.0%, 5.5%, and 4.0%.

The two-temperature model provides an explanation for why the *in-situ* and *ex-situ+RF* Al/Cu bilayer samples have a different thermal response to heating than all other samples. In the in-situ and *ex-situ+RF* Al/Cu samples, the top layer heats up in less than a picosecond (Fig. 4). In other samples, the thermal response time of the top metal layer is on the order of 100 ps (Figs. 4-6). This difference is explained by the strength of the electron-phonon coupling in top vs. bottom layers.

Au and Cu have weak electron-phonon interactions, see Table 1. Fe, Al, and Pt have comparatively strong electron-phonon interactions. In our samples, the Au (weak e-p), Al (strong e-p), and Cu (weak-ep) are top layers. The thermal dynamics of the bilayer are governed by the heat-capacities and thermal conductance between each thermal reservoir, which include the electron-phonon interactions, see Fig. 7. In the ex-situ+RF and in-situ Al/Cu bilayer, the thermal conductance between the Cu electrons, the Al electrons, and the Al phonons is sufficiently high that these three sub-systems effectively form a single thermal reservoir. Alternatively, in Au/Fe and Cu/Pt bilayers, even when the electronic interface conductance is high, the Au-phonons and Cu-phonons take a long time to thermalize with the other sub-systems because Au and Cu have weak electron-phonon coupling. This weak electron-phonon coupling forms a significant thermal resistance. The interplay of electron-phonon coupling, high electron thermal diffusivity, and large phonon heat capacity in metal bilayers was explored in Refs. [24][16]. Our two-temperature modelling results are consistent with the conclusions of these prior works.

We note that the difference in signal in the *ex-situ+RF* Cu/Pt sample arises from a thinner Pt (~4 nm thinner), and not a difference in electronic conductance. Picosecond acoustic signals indicate that the Pt layer is thinner in the *ex-situ+RF* sample, likely as a result of the RF etching prior to the top metal deposition.

Ex-situ preparation of the Au/Fe bilayer leads to a significant reduction in electronic heat transport. Assuming the phonon interface conductance is larger than 0.03 GW m^{-2} K^{-1}, our data suggests the electronic interface conductance is between $0.8 < G_{ee} < 1.9$ GW/(m^2-K), see Fig 8. The electronic conductance is impeded, but not completely.

The *ex-situ* Al/Cu samples have a thermal response that indicates electrons are not able to traverse the metal/metal interface. In the *ex-situ* Al/Cu bilayer, heat takes ~100x as long to traverse the bilayer as compared to the *in situ* and *ex-situ+RF* samples. Our data suggests the electronic conductance is $G_{ee} < 0.08$ GW/(m^2-K). We are unable to place a lower bound on the electron-electron conductance of this sample. Therefore, it is possible the electronic conductance is essentially zero, and all heat is carried across the interface by phonons.

The *ex-situ* Al/Cu sample with different RF etching times indicates that 30 seconds of RF etching time is enough to restore thermal and electronic conductance. Both the 30 sec and 60 second samples have similar thermal response, and their electronic conductance is $G_{ee} > 5$ GW/(m^2-K). The last sample indicates that 10 seconds of RF etching still significantly impedes thermal and electronic conductance, the data suggests the electronic conductance is $G_{ee} < 0.150$ GW/(m^2-K), which is comparable to $G_{ee} < 0.08$ GW/(m^2-K) we observed for the *ex-situ* sample with no RF etching.

We expect exposure of a Cu film to an ambient environment at 100°C will form 1-2 nm of copper oxide [28][29]. The oxide layer is likely Cu_2O, which is a semiconductor [28]. Upon re-loading into the sputtering chamber and being deposited, it is possible that Al reacts will react with the

copper-oxide and form a few monolayers of Al_2O_3. The oxide-interlayer is clearly sufficient to suppress electronic heat-currents, see Fig. 3.

Our results for the interface conductance in the *ex-situ* Al/Cu and Au/Fe bilayers are consistent with prior results for phonon interface conductance values [30]. Similarly, our results for the interface conductance in the *in-situ* and *ex-situ + RF* bilayers are consistent with prior observations of electronic interface conductance [31][32]. Typical phonon interface conductance values are around between $G_{ph} \approx 0.05$ to 0.3 GW/(m^2-K) [30]. The metal/sapphire interface conductance values in our systems are $G_{ph} \approx .265$ GW/(m^2-K), $G_{ph} \approx .085$ GW/(m^2-K), and $G_{ph} \approx .060$ GW/(m^2-K) for the Fe, Cu, and Pt systems, respectively. Alternatively, electronic interface conductances are typically an order of magnitude larger, $G_{ee} > 5$ GW/(m^2-K) [31][32].

If we compare the ex-situ Au/Fe and the ex-situ Al/Cu results, it is surprising to see that the Au/Fe sample has a conductance that is an order of magnitude larger, $G_{ee} \approx 1.7$ GW/(m^2-K) vs. $G_{ee} \approx .065$ GW/(m^2-K). Intuitively, one would assume that the presence of an electrically resistive oxide layer would suppress the electronic conductance to a small value in both systems. This suggests that either the thickness of the Fe oxide layer is not thick enough to prevent electrons from traversing the interface, or that the oxide layer offers only partial coverage.

X-ray photoelectron spectroscopy experiments suggest Fe will form 3-4 nm of oxide in a time-frame of 10 minutes [29]. The oxide is likely to be hematite [29], i.e. Fe_2O_3. Hematite is a poor electrical conductor with a resistivity six to seven orders of magnitude larger than Fe [33]. One possible explanation for the high electron conductance we observe in the *ex-situ* Au/Fe bilayer is the incident Au ions that hit the Fe_2O_3/Fe layer during sputtering of the Au top layer have sufficient kinetic energy to partially dislodge the Fe_2O_3 coating, thereby allowing the Au layer to be in partial contact with the Fe metal layer.

Conclusions

We conducted pump probe measurements and two temperature modeling of thermal transport in Au/Fe, Al/Cu, and Cu/Pt bilayers. We investigate how different preparation of these material systems effects interfacial thermal properties. We show that RF-sputtering metal layers prepared *ex-situ* prior to top metal layer deposition ensures good thermal contact between two metal layers. We show that without an RF surface treatment, the electronic conductance is significantly lowered in the Al/Cu and Au/Fe systems, likely do the formation of Cu and Fe oxide layers. We show that for the Al/Cu system, a minimum of 30 seconds of RF etching time is enough to restore both thermal and electronic conductance. Finally, we show that for the systems that do not form oxides, RF sputtering the *ex-situ* layer does not appear to be necessary to ensure a both a thermally and electrically conductive interface.

Acknowledgements

This work was primarily supported by the NSF (CBET – 1847632). R.W. and F. A. also acknowledge support for sample synthesis by the U.S. Army Research Laboratory and the U.S. Army Research Office under Contract/Grant No. W911NF-18-1-0364 and W911NF-20-1-0274.

Author Declarations

Conflict of Interest

The authors have no conflicts to disclose.

Data Availability

The data that support the findings of this study are available from the corresponding author upon reasonable request.

Table 1: Two temperature model parameters

	Au	Fe	Al	Cu	Ta	Pt	Al_2O_3
Thermal Conductivity Λ_{ph} (W m^{-1} K^{-1})	3[g]	10[a]	10[a]	10[a]	10[a]	7[e]	38
Thermal Conductivity Λ_{el} (W m^{-1} K^{-1})	190[b]	15[b]	250[b]	190[b]	50[b]	2[b]	
Specific Heat C_{ph} (MJ m^{-3} K^{-1})	2.49[f]	3.53	2.42	3.45	2.40	2.84[d]	3.08 [f]
Specific Heat C_{el} (MJ m^{-3} K^{-1})	2.02×10^{4}	2.04×10^{5}	2.80×10^{4}[a1]	3.15×10^{4}[a1]	1.2×10^{5} [a2]	$1.2\times10^{5}5$[a1]	
Electron-Phonon Coupling $g_{el\text{-}ph}$ (W m^{-3} K^{-1})	2.0×10^{16}[h]	100×10^{16}	25×10^{16} [a1]	5.5×10^{16} [a1]	8.8×10^{16}[j]	6.0×10^{17}[c]	
Refractive Index $n+ik$ at 783 nm	.178+ i5.76 [h]	2.89+ i3.32	2.60+ i8.44 [k]	.25+ i5.03	1.1+ i3.5 [k]	2.7+ i5.9[h]	1.77

[a] Reference [36].

[a1] Reference [35].

[a2] Assume to be the same as Pt

[b] Electrical thermal conductivities are determined from the Wiedemann-Franz law and electrical conductivities. Electrical conductivity for each metal was determined via four-point probe measurements of single-layer thin-film samples sputtered separately from the bilayers

[d] Reference [37].

[e] Reference [34].

[f] Reference [38].

[g] Reference [39].

[h] Reference [16]

[j] Reference [40].

[k] Reference [41].

Table 2: Two temperature model parameters for Au/Fe System

	Au/Fe		
Interface Conductance	*in-situ*	*exsitu+RF*	*ex-situ*
G_{ph} (GW m^{-2} K^{-1})	.200 [i]	200 [i]	200 [i]
G_{el} (GW m^{-2} K^{-1})	> 4 [i]	> 4 [i]	1.7 [i]
G_{sub} (GW m^{-2} K^{-1})	.265 [i]	.265 [i]	.265 [i]
Phonon Contribution [%]	99 [i]	99 [i]	99 [i]
Au thickness (nm)	73 nm [j]	74 nm [j]	73 nm [j]
Fe thickness (nm)	17 nm [j]	16 nm [j]	18 nm [j]

[i] Obtained from fitting parameters from thermal analysis.

[j] Obtained from fitting parameters from picosecond acoustics

Table 3: Two temperature model parameters for Al/Cu System

	Al/Cu		
Interface Conductance	*in-situ*	*exsitu+RF*	*exsitu*
G_{ph} [GW/(m^2-K)]	200 [i]	200 [i]	200 [i]
G_{el} [GW/(m^2-K)]	>4 [i]	>4 [i]	.065 [i]
G_{sub} [GW/(m^2-K)]	.080 [i]	.080 [i]	.080 [i]
Phonon Contribution [%]	99 [i]	99 [i]	99 [i]
Al Thickness (nm)	13 nm [j]	14 nm [j]	14 nm [j]
Cu Thickness (nm)	50 nm [j]	52 nm [j]	50 nm [j]

[i] Obtained from fitting parameters from thermal analysis.

[j] Obtained from fitting parameters from picosecond acoustics

Table 4: Two temperature model parameters for Cu/Pt System

	Cu/Pt		
Interface Conductance	*in-situ*	*exsitu+RF*	*ex-situ*
G_{ph} [GW/(m^2-K)]	.200 [i]	200 [i]	200 [i]
G_{el} [GW/(m^2-K)]	3.3-5.6 [i]	3.3-5.6 [i]	3.8-6.5 [i]
G_{sub} [GW/(m^2-K)]	.60 [i]	.060 [i]	.060 [i]
Phonon Contribution [%]	99 [i]	99	99
Cu Thickness (nm)	82	82 nm	82 nm
Pt Thickness (nm)	13 nm	10 nm	13 nm

[i] Obtained from fitting parameters from thermal analysis.

[j] Obtained from fitting parameters from picosecond acoustics

References

[1] B. C. Gundrum, D. G. Cahill, and R. S. Averback, "Thermal conductance of metal-metal interfaces," *Phys. Rev. B - Condens. Matter Mater. Phys.*, vol. 72, no. 24, pp. 1–5, 2005.

[2] M. Hu, P. Keblinski, J. S. Wang, and N. Raravikar, "Interfacial thermal conductance between silicon and a vertical carbon nanotube," *J. Appl. Phys.*, vol. 104, no. 8, 2008.

[3] J. Kimling, A. Philippi-Kobs, J. Jacobsohn, H. P. Oepen, and D. G. Cahill, "Thermal conductance of interfaces with amorphous SiO2 measured by time-resolved magneto-optic Kerr-effect thermometry," *Phys. Rev. B*, vol. 95, no. 18, pp. 1–10, 2017.

[4] A. J. Schellekens, K. C. Kuiper, R. R. J. C. De Wit, and B. Koopmans, "Ultrafast spin-transfer torque driven by femtosecond pulsed-laser excitation," *Nat. Commun.*, vol. 5, pp. 1–7, 2014.

[5] G. M. Choi, B. C. Min, K. J. Lee, and D. G. Cahill, "Spin current generated by thermally driven ultrafast demagnetization," *Nat. Commun.*, vol. 5, pp. 1–8, 2014.

[6] J. Kimling and D. G. Cahill, "Spin diffusion induced by pulsed-laser heating and the role of spin heat accumulation," *Phys. Rev. B*, vol. 95, no. 1, pp. 1–16, 2017.

[7] T. Seifert *et al.*, "Efficient metallic spintronic emitters of ultrabroadband terahertz radiation," *Nat. Photonics*, vol. 10, no. 7, pp. 483–488, 2016.

[8] Z. Feng *et al.*, "Spintronic terahertz emitter," *J. Appl. Phys.*, vol. 129, no. 1, 2021.

[9] B. C. Choi, J. Rudge, K. Jordan, and T. Genet, "Terahertz excitation of spin dynamics in ferromagnetic thin films incorporated in metallic spintronic-THz-emitter," *Appl. Phys. Lett.*, vol. 116, no. 13, 2020.

[10] R. B. Wilson, J. Gorchon, Y. Yang, C. H. Lambert, S. Salahuddin, and J. Bokor, "Ultrafast magnetic switching of GdFeCo with electronic heat currents," *Phys. Rev. B*, vol. 95, no. 18, pp. 1–5, 2017.

[11] K. Jhuria *et al.*, "Spin–orbit torque switching of a ferromagnet with picosecond electrical pulses," *Nat. Electron.*, vol. 3, no. 11, pp. 680–686, 2020.

[12] H. Jang, L. Marnitz, T. Huebner, J. Kimling, T. Kuschel, and D. G. Cahill, "Thermal Conductivity of Oxide Tunnel Barriers in Magnetic Tunnel Junctions Measured by Ultrafast Thermoreflectance and Magneto-Optic Kerr Effect Thermometry," *Phys. Rev. Appl.*, vol. 13, no. 2, p. 1, 2020.

[13] R. B. Wilson and D. G. Cahill, "Experimental validation of the interfacial form of the Wiedemann-Franz law," *Phys. Rev. Lett.*, vol. 108, no. 25, pp. 1–5, 2012.

[14] P. G. Read, "Thermal conductivity," *Gemmol. Instruments*, vol. 52, no. 1, pp. 176–192, 1983.

[15] R. Cheaito *et al.*, "Thermal flux limited electron Kapitza conductance in copper-niobium multilayers," *Appl. Phys. Lett.*, vol. 106, no. 9, 2015.

[16] G. M. Choi, R. B. Wilson, and D. G. Cahill, "Indirect heating of Pt by short-pulse laser

irradiation of Au in a nanoscale Pt/Au bilayer," *Phys. Rev. B - Condens. Matter Mater. Phys.*, vol. 89, no. 6, pp. 1–7, 2014.

[17] J. Kimling, R. B. Wilson, K. Rott, J. Kimling, G. Reiss, and D. G. Cahill, "Spin-dependent thermal transport perpendicular to the planes of Co/Cu multilayers," *Phys. Rev. B - Condens. Matter Mater. Phys.*, vol. 91, no. 14, pp. 1–12, 2015.

[18] D. G. Cahill *et al.*, "Nanoscale thermal transport. II. 2003-2012," *Appl. Phys. Rev.*, vol. 1, no. 1, 2014.

[19] P. E. Hopkins, L. M. Phinney, J. R. Serrano, and T. E. Beechem, "Effects of surface roughness and oxide layer on the thermal boundary conductance at aluminum/silicon interfaces," *2010 14th Int. Heat Transf. Conf. IHTC 14*, vol. 6, pp. 313–319, 2010.

[20] D. W. Oh, S. Kim, J. A. Rogers, D. G. Cahill, and S. Sinha, "Interfacial thermal conductance of transfer-printed metal films," *Adv. Mater.*, vol. 23, no. 43, pp. 5028–5033, 2011.

[21] R. B. Wilson and D. G. Cahill, "Anisotropic failure of Fourier theory in time-domain thermoreflectance experiments," *Nat. Commun.*, vol. 5, pp. 1–11, 2014.

[22] C. Monachon and L. Weber, "Influence of diamond surface termination on thermal boundary conductance between Al and diamond," *J. Appl. Phys.*, vol. 113, no. 18, 2013.

[23] J. Zhu, X. Wu, D. M. Lattery, W. Zheng, and X. Wang, "The Ultrafast Laser Pump-Probe Technique for Thermal Characterization of Materials With Micro/Nanostructures," *Nanoscale Microscale Thermophys. Eng.*, vol. 21, no. 3, pp. 177–198, 2017.

[24] W. Wang and D. G. Cahill, "Limits to thermal transport in nanoscale metal bilayers due to weak electron-phonon coupling in Au and Cu," *Phys. Rev. Lett.*, vol. 109, no. 17, pp. 1–5, 2012.

[25] D. S. Tannhauser, "Conductivity in iron oxides," *J. Phys. Chem. Solids*, vol. 23, no. 1–2, pp. 25–34, 1962.

[26] R. B. Wilson, J. P. Feser, G. T. Hohensee, and D. G. Cahill, "Two-channel model for nonequilibrium thermal transport in pump-probe experiments," *Phys. Rev. B - Condens. Matter Mater. Phys.*, vol. 88, no. 14, pp. 1–11, 2013.

[27] D. G. Cahill, "Analysis of heat flow in layered structures for time-domain thermoreflectance," *Rev. Sci. Instrum.*, vol. 75, no. 12, pp. 5119–5122, 2004.

[28] J. Iijima, J. W. Lim, S. H. Hong, S. Suzuki, K. Mimura, and M. Isshiki, "Native oxidation of ultra high purity Cu bulk and thin films," *Appl. Surf. Sci.*, vol. 253, no. 5, pp. 2825–2829, 2006.

[29] Y. W. S. Suzuki, Y. Ishikawa, M. Isshiki, "Native oxide layers formed on the surface of ultra high-purity iron and copper investigated by angle resolved XPS.," *Materials Transactions, JIM*, vol. 38, no. 111. pp. 1004–1009, 1997.

[30] F. Angeles, Q. Sun, V. H. Ortiz, J. Shi, C. Li, and R. B. Wilson, "Interfacial thermal transport in spin caloritronic material systems," *Phys. Rev. Mater.*, vol. 5, no. 11, p.

114403, Nov. 2021.

[31] R. B. Wilson and D. G. Cahill, “Experimental Validation of the Interfacial Form of the Wiedemann-Franz Law,” *Phys. Rev. Lett.*, vol. 108, no. 25, p. 255901, Jun. 2012.

[32] C. Monachon, L. Weber, and C. Dames, “Thermal Boundary Conductance: A Materials Science Perspective,” *Annu. Rev. Mater. Res.*, vol. 46, no. 1, pp. 433–463, 2016.

[33] G. A. Acket and J. Volger, “Electric transport in N-type Fe2O3,” *Physica*, vol. 32, no. 9, pp. 1543–1550, 1966.

[34] M. J. Duggin, “The thermal conductivities of aluminium and platinum,” *J. Phys. D. Appl. Phys.*, vol. 3, no. 5, pp. 20–23, 1970.

[35] Z. Lin, L. V. Zhigilei, and V. Celli, “Electron-phonon coupling and electron heat capacity of metals under conditions of strong electron-phonon nonequilibrium,” *Phys. Rev. B - Condens. Matter Mater. Phys.*, vol. 77, no. 7, pp. 1–17, 2008.

[36] H. Jang, J. Kimling, and D. G. Cahill, “Nonequilibrium heat transport in Pt and Ru probed by an ultrathin Co thermometer,” *Phys. Rev. B*, vol. 101, no. 6, 2020.

[37] J. W. Arblaster, “The thermodynamic properties of palladium on ITS-90,” *Calphad*, vol. 19, no. 3, pp. 327–337, 1995.

[38] T. P. R. C. Purdue University. Touloukian, Y. S., Air Force Materials Laboratory (U.S.), *Thermophysical properties of high temperature solid materials.* New York: Macmillan, 1967.

[39] G. K. White, S. B. Woods, and M. T. Elford, “The lattice thermal conductivity of dilute alloys of silver and gold,” *Philos. Mag.*, vol. 4, no. 42, pp. 688–692, 1959.

[40] W. H. Butler and O. Ridge, “Electron-phonon interaction effects in tantulum,” vol. 36, no. 8, 1987.

[41] M. A. Ordal, R. J. Bell, R. W. Alexander, L. A. Newquist, and M. R. Querry, “Optical properties of Al, Fe, Ti, Ta, W, and Mo at submillimeter wavelengths,” *Appl. Opt.*, vol. 27, no. 6, p. 1203, 1988.